



# Analytical and numerical analysis of a “springback-forming” process dedicated to stiffened panels

Mohamed El Amine Ait Ali, Dominique Guines, Lionel Leotoing, Eric  
Ragneau

## ► To cite this version:

Mohamed El Amine Ait Ali, Dominique Guines, Lionel Leotoing, Eric Ragneau. Analytical and numerical analysis of a “springback-forming” process dedicated to stiffened panels. International Journal of Mechanical Sciences, 2015, 101-102, pp.399-410. 10.1016/j.ijmecsci.2015.07.031 . hal-01203618

**HAL Id: hal-01203618**

**<https://hal.science/hal-01203618>**

Submitted on 23 Sep 2015

**HAL** is a multi-disciplinary open access archive for the deposit and dissemination of scientific research documents, whether they are published or not. The documents may come from teaching and research institutions in France or abroad, or from public or private research centers.

L'archive ouverte pluridisciplinaire **HAL**, est destinée au dépôt et à la diffusion de documents scientifiques de niveau recherche, publiés ou non, émanant des établissements d'enseignement et de recherche français ou étrangers, des laboratoires publics ou privés.

# Analytical and numerical analysis of a “springback-forming” process dedicated to stiffened panels

M. E. Ait ali<sup>a,b,\*</sup>, D. Guines<sup>a</sup>, L. Leotoing<sup>a</sup>, E. Ragneau<sup>a</sup>

<sup>a</sup> *Université Européenne de Bretagne, INSA de Rennes - LGCGM,  
20, avenue des buttes de coesmes, 35708 Rennes cedex 7, France*

<sup>b</sup> *Université Mohammed V, Ecole Mohammadia d'Ingénieurs - ERD3M,  
20, avenue Ibn sina, 10010 Rabat, Morocco*

---

## Abstract

The aim of this article is to present and to analyze the capabilities of a process named “springback-forming”, dedicated to stiffened panels such as airplane’s fuselage panels. The principle of this forming process is to apply a tension on the stiffener, before the assembly stage with the sheet in a flat configuration using fasteners, adhesives, or a welding process... the bending of the structure is then achieved by springback energy of the stiffener when its tension is released. Using an analytical and finite element models, we studied the capabilities of this process in terms of curvature limits in the case of a single-curved stiffened panel. The results of both models are in good agreement. Through a parametric study, numerical simulations show that when the structure is relatively slender the curvature radius obtained is uniform. Moreover, the value of this radius is independent of the structure’s length and is mainly limited by the stiffener’s height. The carried out experimental tests, using laser beam welding as a joining process, demonstrated the feasibility of the process. From the proposed modeling, it is possible to evaluate the range of achievable curvature radius and its uniformity for different values of both geometrical and mechanical parameters of the structure.

**Keywords:** Stiffened panel, Forming process, Single-curved panel, Springback-forming

---

\*Principal corresponding author

Email address: aitali@emi.ac.ma, Mobile +212654126898 (M. E. Ait ali)

## 1. Introduction

The transportation sector, including aeronautics, automobiles, railway and naval, is based in a large proportion on forming metallic materials. In these sectors, there is a constant need of reducing costs such as: – product development cost (in prototyping or in industrialization stage); – tools cost by making them, for example, more reusable; – manufacturing costs by having less parts and reducing the assembly time. This constant need led to a global approach aiming to have: the most suitable manufacturing processes for each type of parts, and a robust simulation tools to analyze the performance of these processes. In this context, the airplanes manufacturers are interested in the development of innovative forming processes dedicated to stiffened panels such as fuselage panels. These structures are constructed primarily from thin sheets, called also web or skin, and stiffening elements such as beams (Megson, 2010).

An assessment of existing manufacturing technology for metallic fuselage structure was carried out by Pettit et al. (2000). We distinguish, in this assessment, two categories of manufacturing strategy of these stiffened panels: – in the first category, sheets and stiffeners are formed separately and then assembled, mostly by riveting; – in the second category, sheets and stiffeners are first assembled and then formed together to the correct shape.

In the first category, the manufacturing of each element of the structure is based on conventional processes. The most used process for sheets is roll forming to make singly curved panel, as reported by Megson (2010). This process is usually replaced by stretch forming for doubly curved or more complex panels. The stiffeners are extruded or machined and then assembled with the sheet (using bolts, rivets, or a welding process). In this category, the precision of the final shape is mainly dependent on the precision of each component. Furthermore, automatizing of such assembly operations is costly in terms of machines and tools, mainly because of the curvature of the stiffened panels. In contrast, the assembly in flat configuration requires less sophisticated machines and therefore is more cost effective and easier to control.

In the second category, press bend-forming is an effective and often used process, as reported in NASA-CR-124075 (1973). On the one hand, the main advantage of this process is the use of a universal die for all panels; on the

36 other hand, the key problem is the design of the forming path of the punch  
 37 used in the bending process. This issue is often solved by using finite element  
 38 models instead of an experimental approach. Because of the time consuming  
 39 simulations, Yan et al. (2009) developed an equivalent model to improve the  
 40 efficiency of the finite element model and optimize the bend forming path.  
 41 Moreover, the cost of this process increases because of the considerable re-  
 42 alignment work needed to achieve the imposed tolerances (Meyer et al., 1987).  
 43 A more versatile process, in the same category, with lower machine and man-  
 44 ufacturing costs, is shot peen-forming. This process is a major process for  
 45 manufacturing wing skins (Wang and Platts, 2002) and is also used suc-  
 46 cessfully to form fuselage panels (Meyer et al., 1987). Its versatility comes  
 47 from its adaptability to all panel sizes, reduced machines costs since neither  
 48 the die nor the punch is needed, and its good production rate. However,  
 49 with this process only small curvature is achievable and special precautions  
 50 are necessary to avoid producing doubly curved panel. Li (1981) studied  
 51 experimentally the use of pre-bending of the panel while it is formed, using  
 52 peen-forming, as a way to form single-curved stiffened panel. He showed that  
 53 the increase of the pre-bending loads induce the decrease of the curvature  
 54 radius in the pre-bending direction and the increase of the curvature radius  
 55 in the perpendicular direction. Similarly to other processes, to determine the  
 56 process parameters, the trial-and-error approach is more and more replaced  
 57 with efficient numerical models. Wang and Platts (2002) presented a numer-  
 58 ical procedure to obtain the initial blank shape from the final formed surface.  
 59 Garipey (2012) developed a finite element model of the process capable of  
 60 predicting accurately the final shape and the effect of different parameters  
 61 on the process.  
 62 A variation of press bend-forming is warm forming. In this process, the  
 63 bending capability of the panel is extended by increasing the working tem-  
 64 perature, during forming, for an adequate amount of time. Generally, the  
 65 working temperature is around 200 to 300 °C for aluminum alloys (Toro  
 66 et al., 2008). The warm temperature increases the material ductility and  
 67 lowers its yield strength. As a result, smaller curvature radii are achieved  
 68 compared with cold forming processes. However, because of the warming  
 69 equipment necessary additional cost is added.  
 70 A more favored process, in the aerospace industry, is creep age-forming (Lin  
 71 et al., 2006). In this process a heat treatment (artificial aging of aluminum al-  
 72 loys like the 2000 series) takes place, in an autoclave, simultaneously with the  
 73 forming process. The latter is a bend-forming process using vacuum bagging

technique. Holman (1989) showed, by experience, that the smallest residual stresses are obtained using creep age-forming, compared with roll forming, press bend forming, and shot peen-forming. Brewer (1989) tested successfully its feasibility in the case of wing skins and fuselage panels. However, with this process a large springback occurs. An exploratory experimental work was led by Airbus Saint-Nazaire to form a single-curved stiffened panel using this process. The springback varies from 65 to 90%. To help predict the curvature achievable and control the springback, robust numerical models are more and more used. In addition, these models serve to study the feasibility of applying creep age-forming to stiffened panels. Lin et al. (2006) developed a numerical model to estimate the springback of a non-stiffened sheet. The results are between 65 and 80% of the tool's radius. Takafumi et al. (2004) studied experimentally and numerically the forming of doubly-curved stiffened wing skins (using creep age forming). The springback obtained is between 50 and 70% (of the tool's radius) and the difference between the two approaches is less than 7%. Davoodi (2006) studied numerically the forming of a single-curved stiffened panel. The springback obtained is between 65 and 90%.

In this article, we investigate the feasibility of a process that we named "springback-forming". The proposed process: – belongs to the second category; – does not need a die or a punch as in shot peen-forming; – the springback is absent, contrary to the processes mentioned above. To study and analyze the performance of this process, we illustrate its principle in the case of the forming of a single-curved panel with one stiffener. We also developed an analytical and a numerical model to determine the capabilities and the limitations of the process in terms of the achievable curvature radius. We find a good agreement between the two models. We conducted experimental tests, using laser beam welding as a joining process, which demonstrated the feasibility of the process and found a qualitative agreement with numerical model. Hence, using the analytical tool we can evaluate quickly the effect of various parameters on the process.

## 2. Principle and analytical analysis of springback-forming

The objective of this section is to describe the principle of the process and to analyze it using an analytical model. This analytical model allows us to study the effect of geometrical and mechanical parameters on the final shape, and on the residual stresses in the structure after forming.

## 2.1. Principle of the process

In order to illustrate the principle of springback-forming, we consider, in this article, the forming stages of a single-curved stiffened panel. Initially, this stiffened panel contains a rectangular plate and one straight stiffener. Both have the same length and a uniform rectangular cross-section. The stiffener is positioned symmetrically with respect to the plate's width. The springback-forming in this case is composed of three steps:

- Step 1: the stiffener is pre-loaded by a tension force  $\vec{F}$  applied along its neutral axis, Fig. 1.a.
- Step 2: the stiffener and the plate are joined while the stiffener's tension is maintained, Fig. 1.b.
- Step 3: the stiffener's tension  $\vec{F}$  is released, Fig. 1.c.

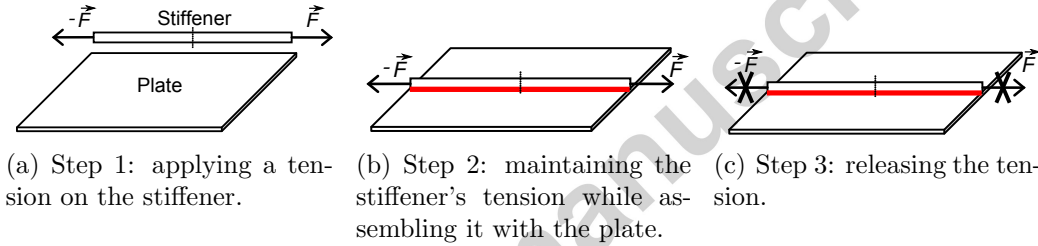


Fig. 1: The three steps of springback-forming.

As described above, this process does not need a die or a punch, the only tool needed is a tool to apply the tension on the stiffener, additionally all the assembly operations are done in a flat configuration. The assembly process (stiffener/plate) could be any process like riveting or welding. Neither the assembly process nor its influence on the forming process is studied in this article.

In step 3, the springback of the stiffener creates a compression load. The resultant of this load is applied in the direction of the stiffener's neutral axis. After the assembly, the centroid of the stiffened panel's cross-section changes (moves toward the plate), thus a bending moment appears in this step. This permanent bending moment allows the forming of the panel. In other words, the springback energy stored in the stiffener allows the forming of the structure.

## 2.2. Analytical model of the process

To evaluate the curvature radius obtained by springback-forming, we develop a model based on the Euler-Bernoulli beam theory. Let's consider the case of the stiffened panel described above in Section 2.1. Fig. 2 shows different geometrical parameters of a cross-section of the assembly (stiffener and plate). Let's denote:

- $y_T$ ,  $y_R$ , and  $y_G$ , the y-coordinate of the cross-section centroid of the plate, the stiffener and the assembly (stiffener and plate);
- $e_T$  and  $B$ , the thickness and the width of the plate;
- $e_R$  and  $h$ , the thickness and the height of the stiffener;
- $S_R$  and  $S_T$ , the cross-sectional area of the stiffener and the plate.

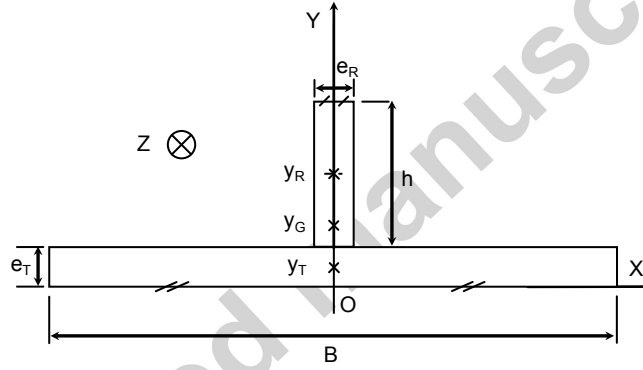


Fig. 2: Geometrical parameters of the assembly's cross-section (stiffener and plate).

In step 3, the bending moment generated is given by the expression:

$$M_{fx} = F(y_R - y_G) \quad (1)$$

In order to use the classical beam theory formulas, the following assumptions are made:

- The assembly between the plate and the stiffener is rigid so no relative displacement is allowed.

- 151 • The assembly process does not introduce any stress field in the struc-  
152 ture.
- 153 • The structure's cross-section dimensions are smaller than its length so  
154 that it might be considered as a beam.
- 155 • The stiffener and the plate's material are the same and this material is  
156 considered homogenous, isotropic, linear, and elastic.
- 157 • The geometrical non-linearities are neglected.

158 Thus, the longitudinal curvature radius (along Z axis) is given by

$$R = \frac{E (I_R^G + I_T^G)}{M_{fx}} \quad (2)$$

159 Where  $I_R^G$  and  $I_T^G$  are the inertia moments of the cross-section of the stiffener  
160 and the plate with respect to the axis  $(G, \vec{X})$  and  $E$  is Young's modulus of  
161 the stiffener and the plate.

162 According to this expression, the panel has a uniform longitudinal curvature.

### 163 2.3. Geometrical analysis

164 The curvature radius's expression, given by Eq. 2, makes it possible  
165 to analyze the effect of the geometrical and mechanical parameters on the  
166 process. First, we have to express it using independent parameters:  $h$ ,  $e_R$ ,  
167  $B$ ,  $e_T$ ,  $E$ , and  $\sigma = F/S_R$  (the tensile stress applied initially to a stiffener's  
168 cross-section). We obtain

$$R = \frac{E (h^4 e_R^2 + 4h^3 e_R B e_T + 6B e_T^2 e_R h^2 + 4h e_R B e_T^3 + B^2 e_T^4)}{6\sigma h e_R B e_T (e_T + h)} \quad (3)$$

169 In order to study the sensibility of the process to different geometrical pa-  
170 rameters, we differentiate the expression given by Eq. 3 with respect to these  
171 parameters to look for optimums. Thus, we obtain

$$\frac{\partial R}{\partial B} = 0 \Leftrightarrow B(R_{min}) = \frac{h^2 e_R}{e_T^2} \quad (4)$$

$$\frac{\partial R}{\partial h} = 0 \Leftrightarrow h(R_{min}) = \frac{e_T (\alpha^2 + e_R^2 - e_R \alpha)}{2e_R \alpha} \quad (5)$$

$$\frac{\partial R}{\partial e_R} = 0 \Leftrightarrow e_R(R_{min}) = \frac{B e_T^2}{h^2} \quad (6)$$

$$\frac{\partial R}{\partial e_T} = 0 \Leftrightarrow e_T(R_{min}) = \frac{h (\beta^2 + B^2 - B\beta)}{2B\beta} \quad (7)$$



172 where

$$\alpha = \left( e_R^2 \left( 2B + 2\sqrt{B(B - e_R)} - e_R \right) \right)^{\frac{1}{3}}$$

$$\text{and } \beta = \left( B^2 \left( 2e_R + 2\sqrt{e_R(e_R - B)} - B \right) \right)^{\frac{1}{3}}$$

173 These minima ( $B(R_{min})$ ,  $h(R_{min})$ ,  $e_R(R_{min})$ , and  $e_T(R_{min})$ ) does not always  
 174 correspond to realistic stiffened panels dimensions. However, they are the  
 175 reference for the minimum curvature radius achievable for any configuration.  
 176 For example, if we fix all the parameters except the stiffener's height, then the  
 177 smallest curvature radius achievable with this process, for this structure, is  
 178 obtained when  $h = h(R_{min})$ . On the other hand, it is interesting to observe  
 179 that the expression of these minima depends only on the geometry of the  
 180 structure, and does not depend on the initial tensile stress, which could be  
 181 useful during the design of such structures.

182 To further understand the existence of these minima, let's consider Eq. 2.  
 183 When a parameter varies, the inertia moment of the cross-section and the  
 184 bending moment (Eq. 1) are also modified. Both of these quantities depend  
 185 on  $y_G$ . The expression of  $y_G$  is given by:

$$y_G = \frac{Be_T^2 + 2he_R e_T + h^2 e_R}{2(he_R + Be_T)} \quad (8)$$

186 We note that when  $B = B(R_{min})$  or  $e_R = e_R(R_{min})$ , we have  $y_G = e_T$ , which  
 187 means that the cross-section centroid is at the interface stiffener-plate. It is  
 188 worth noting that this observation is not valid when  $h = h(R_{min})$  or when  
 189  $e_T = e_T(R_{min})$ .

190 Another way to demonstrate the existence of these minima is by considering  
 191 the extreme values of each parameter:

- 192 1. For the plate's width  $B$ ,  $B \mapsto 0$  is equivalent to the case where there  
 193 is no plate. After the release of the stiffener, the latter will not bend,  
 194 hence  $R = \infty$ . Similarly, if  $B \mapsto +\infty$ , the plate's inertia moment ap-  
 195 proaches infinity but the bending moment  $M_{fx}$  remains finite. There-  
 196 fore, considering Eq. 2,  $R = \infty$ , which demonstrates the existence of a  
 197 value of  $B$  that gives a minimum value of  $R$ .
- 198 2. In the case of the stiffener's thickness  $e_R$ ,  $e_R \mapsto 0$  is equivalent to a  
 199 panel without a stiffener, so the plate stays flat, thus  $R = \infty$ . Using  
 200 the same argument when  $e_R \mapsto +\infty$  as when  $B \mapsto +\infty$ , we deduce the  
 201 existence of a value of  $e_R$  that gives a minimum value of  $R$ .

- 202 3. Let's consider now the extreme values of the stiffener's height  $h$ .  $h \mapsto 0$   
 203 is equivalent to a structure with only a plate, so it stays flat, this means  
 204  $R = \infty$ . However, if  $h \mapsto +\infty$ , the bending moments  $M_{fx} \mapsto 0$  ac-  
 205 cording to Eq. 1. Moreover, the stiffener's inertia moment approaches  
 206 infinity ( $h$  is cubed in this inertia moment), and considering Eq. 2 we  
 207 deduce that  $R = \infty$ . In the same way, we conclude that there is a value  
 208 of  $h$  that gives a minimum value of  $R$ .
- 209 4. For the plate's thickness  $e_T$ ,  $e_T \mapsto 0$  is equivalent to saying that there  
 210 is no plate. As in the case of the plate's width, the stiffener will not  
 211 bend, so  $R = \infty$ . However, when  $e_T \mapsto +\infty$ , the bending moment  
 212 generated will increase linearly with  $e_T$ , but the plate's inertia moment  
 213 will increase more rapidly, as its expression contains the term  $e_T^3$ . Tak-  
 214 ing into account Eq. 2, we deduce that  $R = \infty$  and hence the existence  
 215 of minimal value of  $R$  for a certain value of  $e_T$ .

#### 217 2.4. Mechanical analysis

218 Mechanical analysis of the process concerns: (i) the effect of the material's  
 219 Young's modulus on the process (ii) and investigations of stress distribution  
 220 in the structure at different stages of the process.

221 For given fixed dimensions of the structure, according to the curvature radius  
 222 expression, Eq. 2, the smaller the material's stiffness (stiffener and/or plate),  
 223 the smaller the curvature radius achieved.

224 As for the stresses induced in the structure, when the pre-load  $F$  is applied  
 225 during step 1 of the process, a positive tensile stress  $\sigma^1 = F/S_R$  is generated  
 226 in the stiffener. The plate is supposed to be initially free of stress. In step 2,  
 227 we supposed (in Section 2.2) that the assembly process does not introduce  
 228 any stress field in the structure. In step 3, releasing the tension force is  
 229 equivalent to applying, in both the stiffener and the plate, a compression  
 230 stress  $\sigma_{Compr}^3 = -S_R\sigma^1/(S_R + S_T)$  and a bending stress  $\sigma_{Bend}^3 = -M_{fx}(y -$   
 231  $y_G)/(I_R^G + I_T^G)$ .  $M_{fx}$  is the bending moment given by Eq. 1 and  $y$  is the  
 232 y-coordinate of a point of the considered cross-section (see Fig. 2). By  
 233 applying the superposition principle, we deduce the residual stress  $\sigma_{Res}$  in  
 234 the cross-section of the structure after forming:

$$\begin{aligned}\sigma_{Res} &= \sigma^1 + \sigma_{Compr}^3 + \sigma_{Bend}^3 \\ &= \sigma^1 - \frac{S_R}{S_R + S_T}\sigma^1 - M_{fx}(y - y_G)/(I_R^G + I_T^G)\end{aligned}\quad (9)$$

Fig. 3 shows the normal stresses in a cross-section of a stiffened panel formed using springback-forming. This stiffened panel is composed of a plate with a rectangular cross-section ( $B = 170\text{ mm}$ ,  $e_T = 2.4\text{ mm}$ ) and a stiffener with a rectangular cross-section ( $e_R = 2.4\text{ mm}$ ,  $h = 17.5\text{ mm}$ ). The material's Young's modulus of both parts is  $70500\text{ MPa}$  and the initial tensile stress applied  $\sigma^1 = 218\text{ MPa}$ . The figure also shows stress levels in the structure

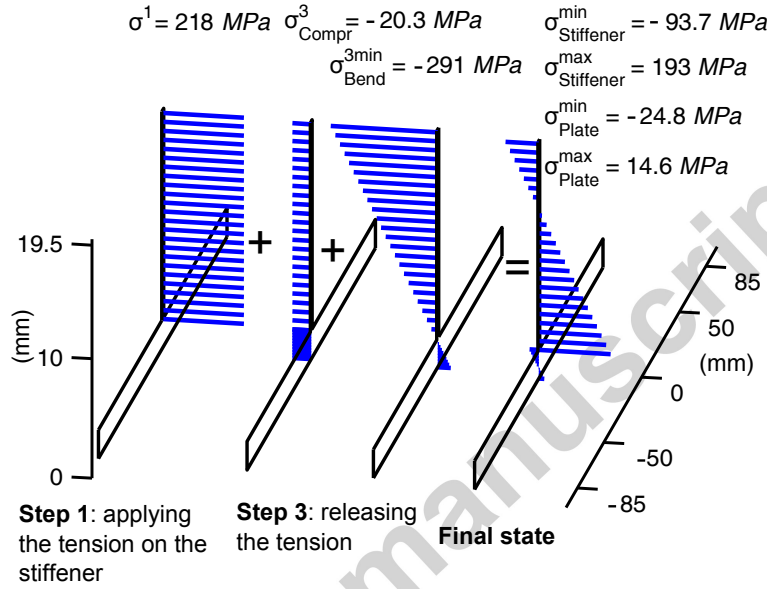


Fig. 3: Example of residual stresses in the structure after its forming by springback-forming.

at each step of the process. We note that the maximum residual stress ( $193\text{ MPa}$ ), after forming, is located at the base of the stiffener (interface stiffener-plate). In this particular example, this value is smaller than the initial applied stress; however, it could be higher in certain cases. On the other hand, in the plate we note the existence of a typical bending stress profile because the cross-section centroid is located in the plate's thickness. Otherwise, when this centroid is in the stiffener, we could have only tensile or compressive stresses in the plate. In any case, we note that the plate's stress levels are smaller compared with the initial tensile stress. Furthermore, as we supposed that the plate is stress free in step 1, we observe a stress discontinuity at the interface stiffener-plate; hence, a shearing stress will occur

at this interface.

In this article, we neglected the effects of the assembly process on springback-forming. However, some of these effects are already considered in the analytical analysis presented in this section. Indeed, using riveting or bolting as a joining process requires drilling holes and use of a flange or a parallel area to the plate. In any case, it means that the cross-section geometry of the plate or the stiffener or both of them has changed. These changes are considered through the bending moment formula, Eq. 1, and the longitudinal curvature radius expression Eq. 2. The stress distribution change in the structure will be partially considered by the residual stress equation, Eq. 9. However, in and nearby every cross-section where rivets or bolts are used, the stress distribution will slightly change and higher stresses values will concentrate near the drilled holes.

On the other hand, using welding as a joining process introduces, in the structure, distortions and a residual stress field that interacts with the pre-stress applied to the stiffener. These distortions and the distribution of residual stress are complex. They require a detailed study to analyze their effect on the process. Such a study is beyond the scope of this article and will be treated in another publication.

### 3. Numerical simulation of springback-forming

In this section, we present a finite element (FE) model developed in Abaqus (6.8) software environment to study the forming of a stiffened panel by springback-forming. With this numerical model, we were able to integrate the geometric and material non-linearities and also to obtain a more realistic distribution of residual stresses, particularly in the plate.

#### 3.1. Finite element model presentation

The stiffened panel simulated, in this paragraph, has a cross-section similar to the example studied in the mechanical analysis Section 2.4. The parts length is  $4m$ . Both are made from an isotropic aluminum alloy 6056 *T4* with a Young's modulus  $E = 70500 MPa$ , a Poisson ratio  $\nu = 0.33$ , and a flow curve extracted from Davoodi (2006) and presented in Fig. 4. The initial tensile stress applied to the stiffener is  $\sigma^1 = 300 MPa$ .

Taking into account the pre-strain dependence of the Young's modulus would increase the quantitative accuracy of the model. However, it would not change the qualitative conclusions. As the biggest strain applied in all the

simulations did not exceed 4% and to keep the model simple, we neglected this dependence.

We assumed that the material follow an elasto-plastic law with isotropic hardening behavior (Von Mises plasticity model). The springback calculation accuracy is highly influenced by Bauschinger effect, but only when the material undergoes a complicated cyclic deformation; which is note the case in springback-forming. In addition, no reverse yielding will occur in all the simulations carried out in this article. For these two reasons, we neglected the Bauschinger effect and the influence of the yields-locus of the material.

Considering the longitudinal symmetry only half of the structure's length is

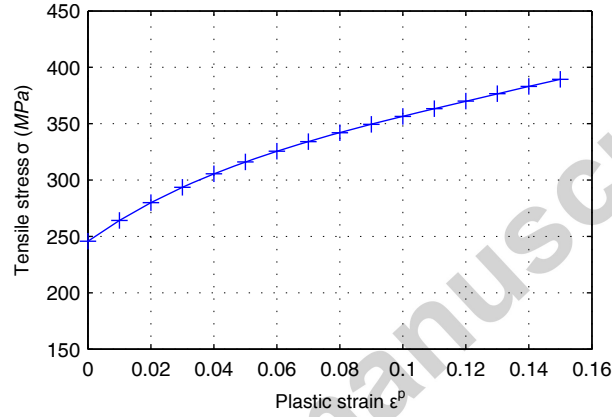


Fig. 4: Hardening curve of the aluminum alloy 6056 *T*4 at 20°C (Davoodi, 2006).

modeled. The geometrical non-linearities are taken into account. To mesh the structure, we used shell elements S4R (4 nodes and a reduced integration), issued from the elements library of Abaqus. In all the simulations carried in this work, the size of the elements is  $\simeq 2\text{ mm} \times 2\text{ mm}$  in the stiffener and is  $\simeq 4\text{ mm} \times 4\text{ mm}$  in the plate. Fig. 5 shows an example of such mesh.

The assembly stiffener-plate is modeled as rigid constraint between the edges in contact. The simulation consist of three static steps: (i) applying the tension on the stiffener, (ii) activating the rigid constraint, (iii) and finally releasing gradually the stiffener's tension.

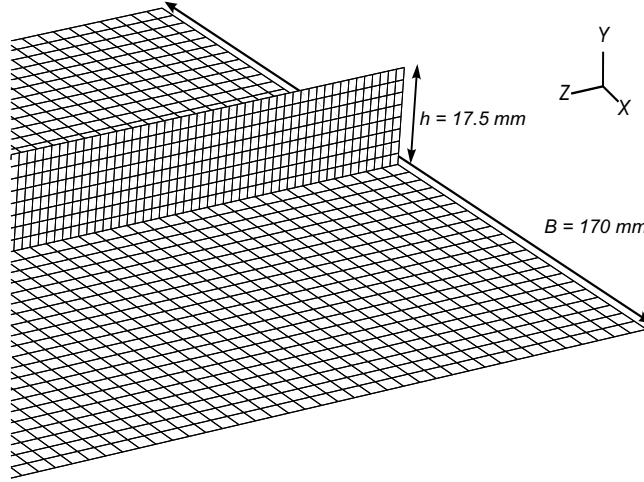


Fig. 5: Example of mesh used in the finite element model.

### 3.2. Curvature characterization

As we are interested in the curvature radius, we need a detailed analysis of this radius in every point of the panel. So, after forming, the plate is discretized into  $m$  longitudinal fibers (Fig. 6.b) parallel to the stiffener. The position of a fiber  $j$  ( $j = 1, ..m$ ) along the X-direction is noted  $x_j$ . Each fiber is discretized into  $n$  points  $M_{i=1,..n}$ . To calculate the curvature radius  $R(x_j)$  of a fiber  $j$ , we fit a circular segment by minimising

$$\Delta(R, O) = \sum_{i=1}^n \left( R - \|\overrightarrow{OM_i}\| \right)^2 \quad (10)$$

where  $O$  is the circle's center, which is in the longitudinal symmetry plane  $Z = 0$  of the plate. Once we determine the couple  $(R(x_j), O(x_j))$ , we define a radial error for the fiber  $j$  (in  $mm$  unit like a dimensional tolerance)

$$error(x_j) = \max_{i=1,n} \left( |R(x_j) - \|\overrightarrow{O(x_j)M_i}\|| \right) \quad (11)$$

which indicates the degree of uniformity of the fiber's curvature (Fig. 6.a). So, for each panel we can plot the transverse variation of the curvature radius and the radial error versus the fibers' position  $x_j$  (Fig. 6.b). To have a global characteristic of the panel's curvature, we define the transverse dispersion

$$\Delta R = R_{max} - R_{min} \quad (12)$$

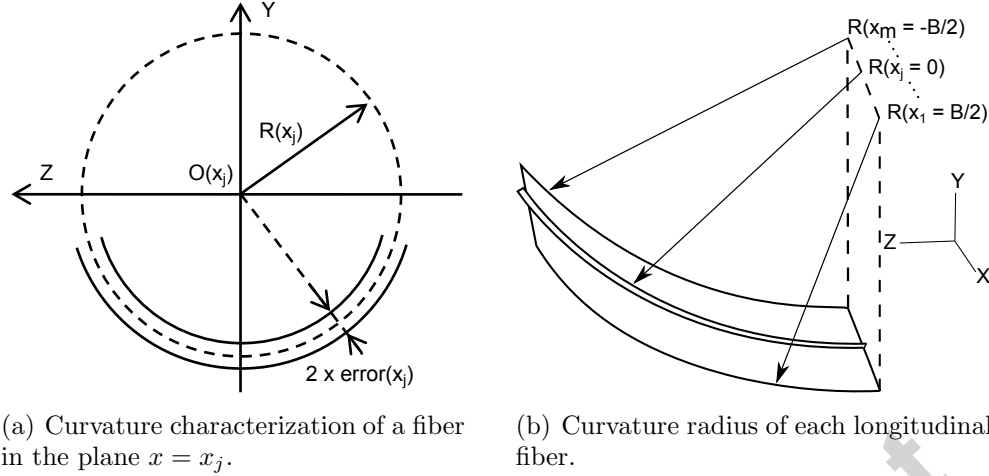


Fig. 6: Characterization of the longitudinal curvature of a panel.

where  $R_{max}$  and  $R_{min}$  are the maximum and the minimum value of  $R$ . Thus, for a panel, we dispose of three characteristics: (i) the curvature radius of the plate's longitudinal center fiber (the one in contact with the stiffener), (ii) the transverse dispersion  $\Delta R$ , (iii) and the maximum of the radial errors.

### 3.3. Deformation, curvature radius and residual stresses after forming

We simulated the case defined in the model presentation Section 3.1. The deformation of the plate after forming is shown by displacement of its nodes in Fig. 7. Far from the plate's ends, the transverse displacement distribution is relatively uniform along its length, Fig. 7.a. However, the maximum amplitude is negligible ( $\leq 0.014\text{ mm}$ ). On the other hand, no noticeable deflection of the plate's corners is observed in Fig. 7.b and Fig. 7.c. Following the definitions of the previous section, Fig. 8 shows the detailed analysis of the panel's curvature radius. We note that the radial error, in all the panel, is inferior to  $0.2\text{ mm}$ , which indicates that the curvature radius is quit uniform in every sheet's fiber. Moreover, the transverse dispersion  $\Delta R$  is inferior to  $0.3\text{ mm}$ , which indicates that the panel has a good uniformity of its curvature radius.

Fig. 9 shows the longitudinal residual stress distribution in the stiffener after forming (the other components of the Cauchy tensor stress are negligible). We see that the higher stresses are located near the interface stiffener-plate.

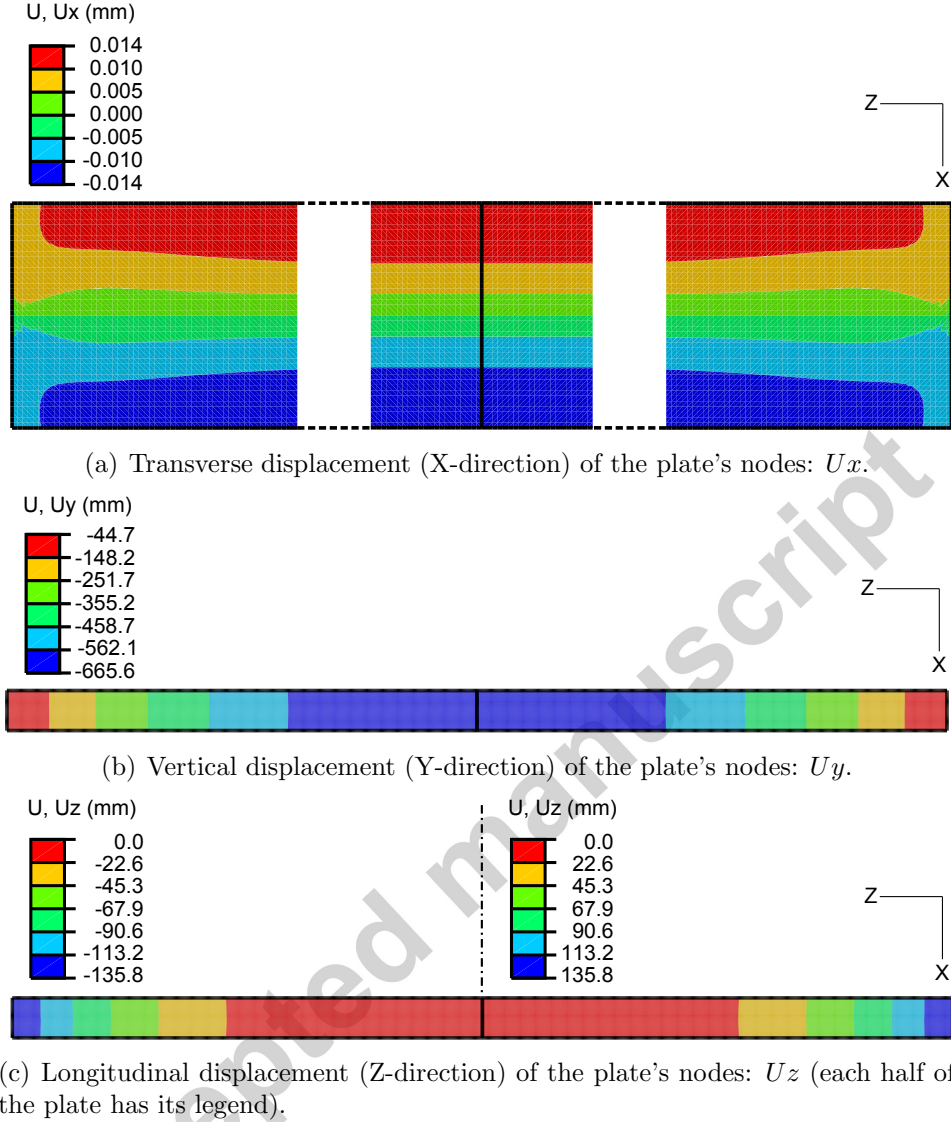


Fig. 7: Plate's nodes displacement after forming by springback-forming (plate:  $4\text{ m} \times 170\text{ mm} \times 2.4\text{ mm}$ , stiffener:  $4\text{ m} \times 17.5\text{ mm} \times 2.4\text{ mm}$ , initial applied stress  $\sigma^1 = 300\text{ MPa}$ ).

342 To illustrate the distribution of the stresses in a stiffener's cross-section,  
 343 Fig. 10.a shows the principal stresses of the stiffener's middle section (plane  
 344  $Z = 0$ ) obtained using the FE model. To compare it to the analytical model's  
 345 results, Fig. 10.b shows the stresses obtained by the analytical model (Section



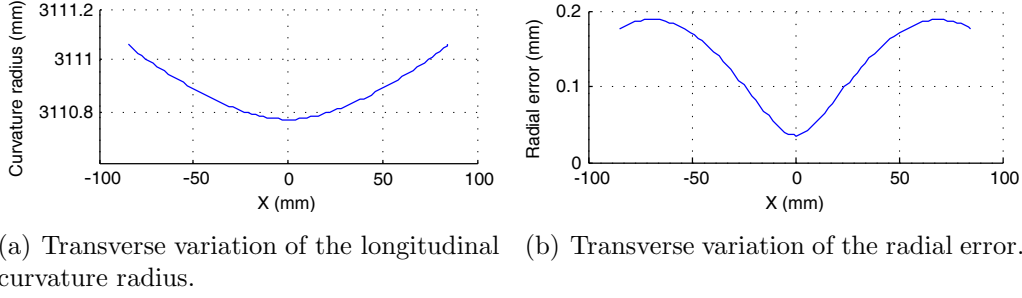


Fig. 8: Curvature characterization of a panel after forming by springback-forming (plate:  $4\text{ m} \times 170\text{ mm} \times 2.4\text{ mm}$ , stiffener:  $4\text{ m} \times 17.5\text{ mm} \times 2.4\text{ mm}$ , initial applied stress  $\sigma^1 = 300\text{ MPa}$ ).

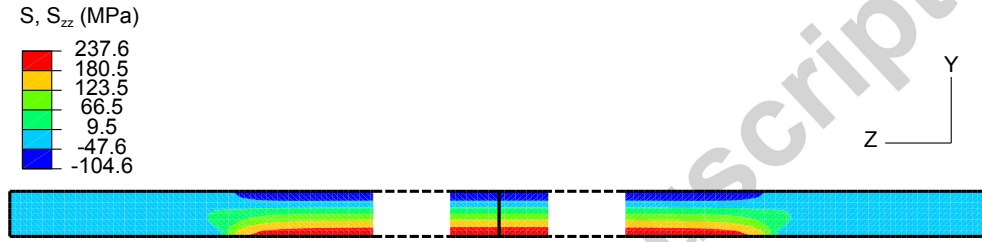


Fig. 9: Longitudinal residual stress in the stiffener after forming.

2.4) as well as extreme stress values in the stiffener and in the plate. We note that there is a good qualitative correlation between the results. The principal stresses of the plate's middle section ( $Z = 0$ ) obtained using the FE model are shown in Fig. 11. We note that, as in the stiffener, the longitudinal stresses are dominant. Though the analytical model predicts a constant stress along the X-direction in the plate's cross-section, as shown by Fig. 10.b, the FE model shows a variation  $\leq 16\text{ MPa}$  of this stress. However, we note that they are of the same nature as the analytical stresses (compressive stresses in sheet's superior surface and tensile stresses on the other surface). To evaluate the stress field in the plate, Fig. 12 shows the distribution of the Von Mises stress in both its superior and inferior surfaces. We observe that far from a limited zone near the plate's ends, in contact with the stiffener, the stress level does not exceed  $54\text{ MPa}$ . As shown in Fig. 9 and Fig. 12, we note also that far from the plate's ends, the spatial distribution of residual stresses is relatively uniform along the length of the structure.

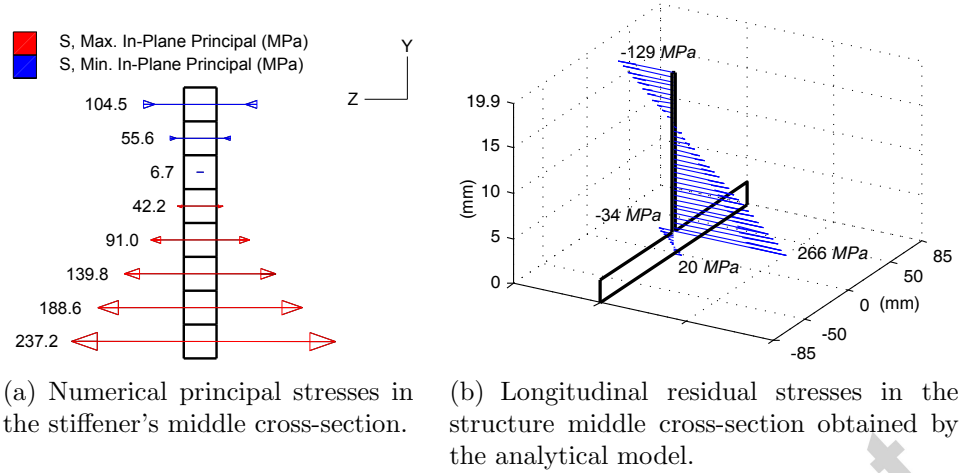


Fig. 10: Principal stresses in a structure's middle cross-section after forming.

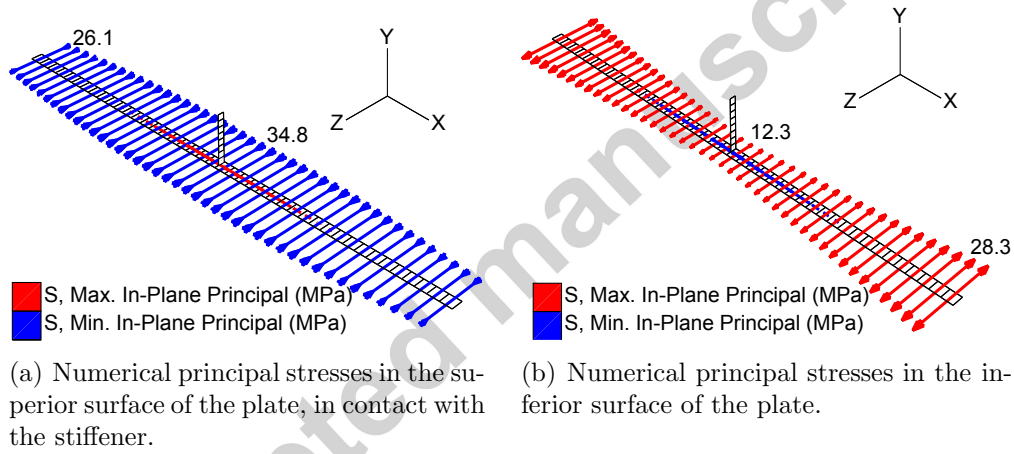


Fig. 11: Principal stresses in the central transverse section of the plate after forming.

#### 4. Parametrical analysis and an experimental test of springback-forming

We consider the structure geometry described in Section 3.3 as a reference configuration. Using the FE model, we study in this section, the curvature radius variation with respect to one mechanical parameter: the initial stiffener's tensile stress  $\sigma^1$ ; and with respect to three geometrical parameters:

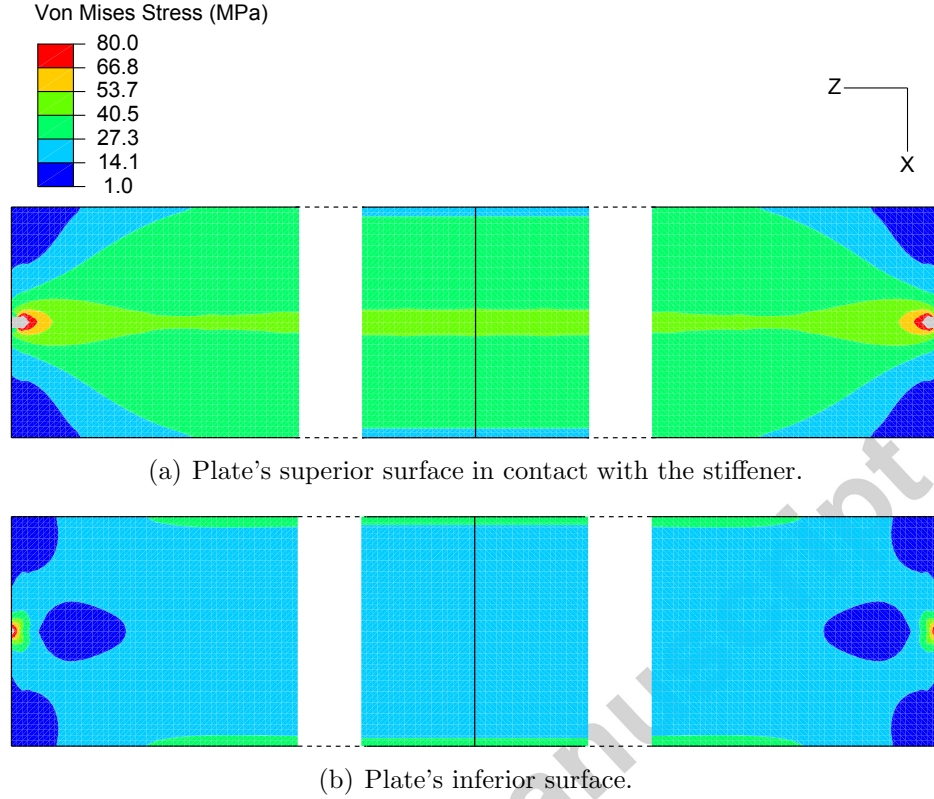


Fig. 12: Von Mises stresses in the plate after its forming by springback-forming.

stiffener's height  $h$ , plate's width  $B$ , and structure's length  $L$ . For each parameter variation, numerical to analytical results are compared. In addition, we present the results of three experimental tests of springback-forming.

#### 4.1. Initial stiffener's tension effect

To analyze the effect of the initial stiffener's tension, different pre-load values, ranging from  $6\text{ kN}$  to  $12.1\text{ kN}$ , were applied on the stiffener. These pre-loads induce stresses below and above the material's yield point (Fig. 4). Some stress values with the corresponding applied forces and longitudinal strains are given in Table 1.

Fig. 13 gives the variation of the curvature radius of the plate's longitudinal center fiber, obtained by the numerical and the analytical model, with respect to the stiffener's initial tensile stress. In all the simulations, the ra-

Tensile stress $\sigma^1$ (MPa)	142	219	246	254	300
Elastic strain $\epsilon_{zz}^e$ (%)	0.2	0.31	0.35	0.36	0.43
Plastic strain $\epsilon_{zz}^p$ (%)	0	0	0.02	0.45	3.54
Applied force ( $kN$ )	6	9.2	10.3	10.6	12.1

Table 1: Initial loads and corresponding tensile stresses applied to the stiffener ( $4m \times 17.5mm \times 2.4mm$ ).

379 dial error is inferior to  $0.2mm$ , which indicates that the curvature radius is  
 380 uniform in every plate's fiber. Additionally, the transverse dispersion  $\Delta R$   
 381 is inferior to  $0.36mm$ , which indicates that the panel, in every case, have a  
 382 good uniformity of its curvature radius. On the other hand, the results of  
 both models are very similar, as the difference is inferior to  $0.4\%$ . This small

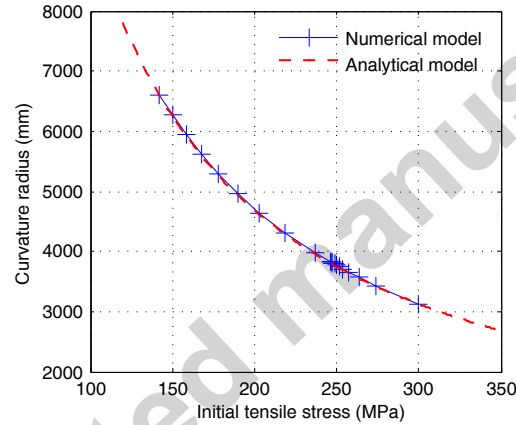


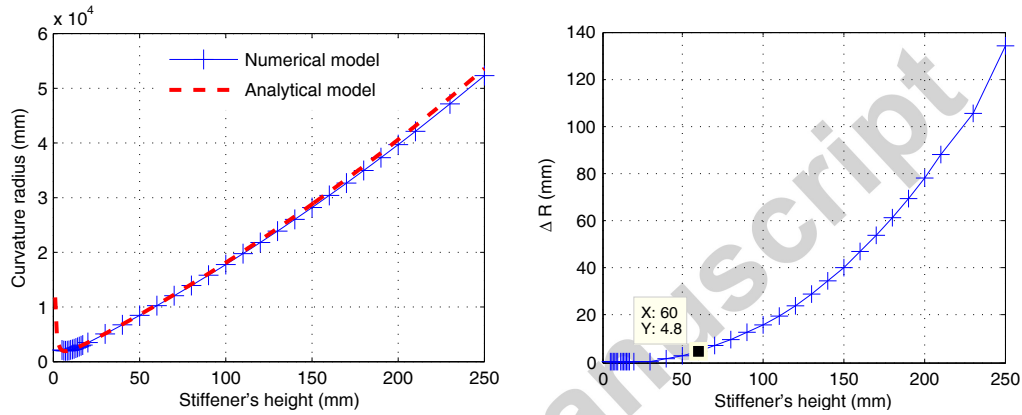
Fig. 13: Variation of the plate's curvature radius with respect to the initial tensile stress applied to the stiffener.

383 difference shows that, for this structure, the analytical model gives a good  
 384 estimation of the curvature radius.  
 385

#### 386 4.2. Stiffener height's effect

387 For this study, the stiffener's height varies from  $6$  to  $250mm$ ; but, the  
 388 other parameters are the ones of the reference configuration ( $e_R = e_T =$   
 389  $2.4mm$ ,  $B = 170mm$ ,  $L = 4000mm$ , and  $\sigma^1 = 300MPa$ ).

390 The results of the simulations are synthesized in Fig. 14. The radial error,  
 391 in all these simulations, is inferior to  $0.4\text{ mm}$ , which indicates the uniformity  
 392 of the curvature radius of all the plate's longitudinal fibers. We note, ad-  
 393 ditionally, in Fig. 14.a, that both curves (analytical and numerical) have a  
 394 minimum value of the plates' curvature radius when  $h(R_{min}) = 7\text{ mm}$ . We  
 395 note also that the curvature radius increases significantly with the increas-  
 396 ing of the stiffener's height (more than  $1.3\text{ m}$  for every  $10\text{ mm}$  increase of  
 397  $h$ ). This result could be a limitation of the use of springback-forming for  
 stiffened panels with high height stiffeners.



(a) Variation of the curvature radius of the plate's longitudinal center fiber with respect to the stiffener's height. (b) Variation of the curvature radius's transverse dispersion ( $\Delta R = R_{max} - R_{min}$ ) in the plate with respect to the stiffener's height.

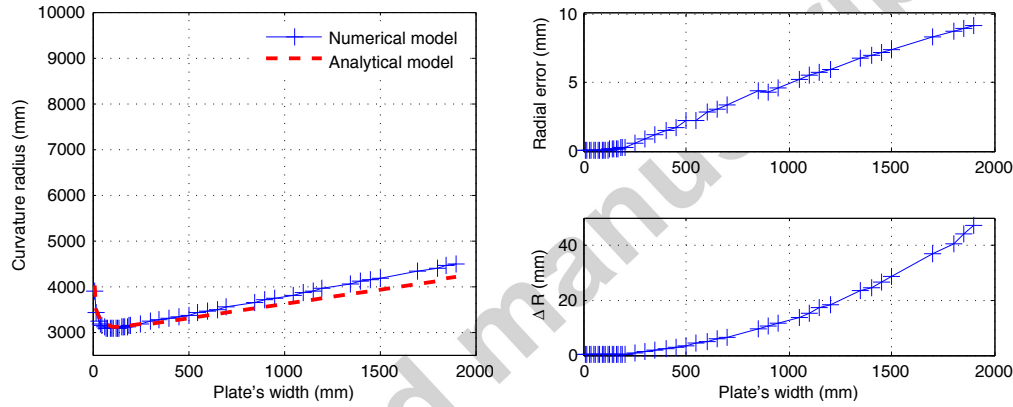
Fig. 14: Stiffener's height effect on the plate's curvature radius after forming.

398 Moreover, we observe a good agreement between numerical and analytical  
 399 results, as the difference is inferior to 2.3%. However, as shown in Fig.  
 400 14.b, the transverse dispersion of the curvature radius, which is absent in  
 401 the analytical model, increases with the stiffener's height. Relatively to the  
 402 curvature radius this dispersion is inferior to 0.3%. But this dispersion could  
 403 be unacceptable during the assembly of the stiffened panel with an other  
 404 structure. In case of an imposed tolerance on the curvature radius uniformity,  
 405 the curve presented in Fig. 14.b. would be used to determine the maximum  
 406 value of  $h$ , for which with springback-forming that tolerance will be respected.  
 407

#### 4.3. Plate width's effect

The capability of the springback-forming to impose a uniform curvature radius on a given plate's width is important. Indeed, it has a direct impact on how many stiffeners should be used to form a larger panel, and expect to have a uniform curvature radius. To study the effect of the plate's width on the process, we fixed the rest of the parameters to those of the reference configuration ( $e_R = e_T = 2.4 \text{ mm}$ ,  $h = 17.5 \text{ mm}$ ,  $L = 4000 \text{ mm}$ , and  $\sigma^1 = 300 \text{ MPa}$ ) and we varied  $B$  from  $10 \text{ mm}$  to  $1800 \text{ mm}$ .

The variation of the curvature radius (of the plate's longitudinal center fiber) versus the plate's width, obtained with both models (numerical and analytical), is given in Fig. 15.a. We note a relatively good agreement between the numerical and analytical results, as the difference is inferior to 2.3%.



(a) Variation of the curvature radius of the plate's longitudinal central fiber with respect to the plate's width.

(b) Variation of curvature radius's transverse dispersion ( $\Delta R = R_{max} - R_{min}$ ) and the radial error in the plate with respect to the plate's width.

Fig. 15: Plate's width effect on its curvature radius after forming.

The same figure shows the existence of a minimum value around  $B(R_{min}) = 110 \text{ mm}$ . In Fig. 15.b, we note that the radial error and the transverse dispersion increase with the plate's width. This increase indicates a decrease of both the longitudinal and transversal uniformity of the curvature radius. We observe the same tendencies as with stiffener's height. However, the width's plate has a weaker effect (than the stiffener's height) on the curvature

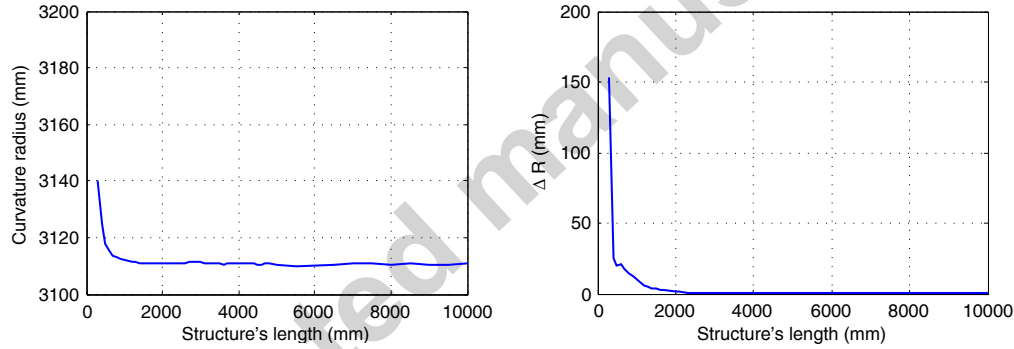
radius. Indeed, there is a variation of less than  $2\text{ m}$  for a width variation of  $1800\text{ mm}$ .

On the other hand, we conclude that for plate's widths inferior to  $B_{lim} = 200\text{ mm}$ , the uniformity of the curvature radius is excellent (radial error  $\leq 0.3\text{ mm}$ , transverse dispersion  $\leq 0.4\text{ mm}$ ). In case of an imposed tolerance on the curvature radius uniformity, the transverse dispersion curve presented in Fig. 15.b would be used to determine the maximum value of  $B$ , for which with springback-forming that tolerance will be respected.

#### 4.4. Structure length's effect

To study the effect of the structure's length on the curvature radius, we considered the reference configuration dimensions ( $h = 17.5\text{ mm}$ ,  $e_R = e_T = 2.4\text{ mm}$ ,  $B = 170\text{ mm}$ , and  $\sigma^1 = 300\text{ MPa}$ ) and we changed the length from  $0.3\text{ m}$  to  $10\text{ m}$  with a step of  $100\text{ mm}$  up to  $5\text{ m}$  and a step of  $500\text{ mm}$  up to  $10\text{ m}$ .

Fig. 16.a shows the variation of the curvature radius of the plate's longitudinal center fiber for different structure's length. In all the simulations the



(a) Variation of the curvature radius of the plate's central fiber with respect to the structure's length.

(b) Variation of the curvature radius's transverse dispersion ( $\Delta R = R_{max} - R_{min}$ ) in the plate with respect to the structure's length.

Fig. 16: Structure's length effect on the plate's curvature radius after forming.

radial error is inferior to  $0.3\text{ mm}$ , which indicates that the curvature radius is uniform in all plate's longitudinal fibers. We note that the value of the curvature radius is quasi-constant for all the lengths, as the variation is inferior to  $40\text{ mm}$ . However, the transverse dispersion is greater for small values

of the structure's length (up to  $150\text{ mm}$ ), Fig. 16.b.

We also note, in Fig. 16, that when the structure is long enough (length  $\geq 2\text{ m}$ ) compared with structure's cross-section dimensions, the curvature radius value becomes constant ( $\pm 0.5\text{ mm}$ ) and the transverse dispersion becomes small ( $\leq 1.4\text{ mm}$ ). In other words, the curvature radius becomes independent of the initial structure's length.

#### 4.5. An experimental test of springback-forming

To test the feasibility of springback-forming experimentally, we conducted three forming tests. The objective of these tests is: – to demonstrate the capability of the process to bend a single-curved structure; – to show the repeatability of the results; – to test the sensibility of the process to the initial stiffener's tension; – and to compare the curvature radius obtained numerically and experimentally.

The geometry and the material of the structure, in the three tests, is the same as in the mechanical analysis Section 2.4. As we showed that the results of bending using springback-forming are independent of the structure's length, we chose the plates length  $355\text{ mm}$  and the stiffeners length  $541\text{ mm}$ . The additional length of the stiffeners is necessary to allow the use of grips to apply tension during the first phase of the forming process. The thickness of all parts is  $2.4\text{ mm}$  and the plates width is  $170\text{ mm}$ . The rest of the characteristics of the tests is given in Table 2.

	Test 1	Test 2	Test 3
Stiffeners height ( $\text{mm}$ )	17.5	17.6	17.5
Initial tensile stress $\sigma^1$ (MPa)	214.2	202.2	155.3

Table 2: Stiffeners height and the initial tensile stress applied to them in the three experimental tests of springback-forming.

As a joining process, welding is more challenging than riveting or bolting to integrate in springback-forming. Nevertheless, it helps reducing the structure mass by simplifying the interface between the stiffeners and the plate. It is also easy to automate and easily adaptable to complex geometries. For these reasons, we used laser beam welding as a joining process in the experiments. We used a YAG welding source to form a tee joint between the stiffener and the plate without a filler material. The laser beam was focused in the plate's



inferior surface, perpendicular to the plate, positioned above and in the opposite side of the stiffener; and had a diameter of  $0.2\text{ mm}$ , a travelling speed of  $0.6\text{ m/minute}$  and a power of  $1700\text{ W}$ . This welding configuration was used to keep the longitudinal symmetry of the structure. As a shielding gas, we used argon with a flow rate of  $20\text{ liter/minute}$ . With the imposed welding parameters, we obtained a welding bead with little porosity, a uniform width and no visible fissures. In addition, the fusion zone included a part from the stiffener throughout its length.

To measure the geometrical shape of the structure after forming, we used a coordinate measuring machine with a sphere as probe. As we are interested in the longitudinal curvature, we measured the points' coordinates of 17 fibers equally spaced along the width of the plate and parallel to the stiffener. Each fiber was composed of 70 points equally spaced. The precision of coordinate measures, using a sphere as probe, was quite good:  $10^{-3}\text{ mm}$  for X-coordinates,  $10^{-2}\text{ mm}$  for Y-coordinates and  $10^{-1}\text{ mm}$  for Z-coordinates. A result of this measuring procedure applied to Test 2 is given in Fig.17.

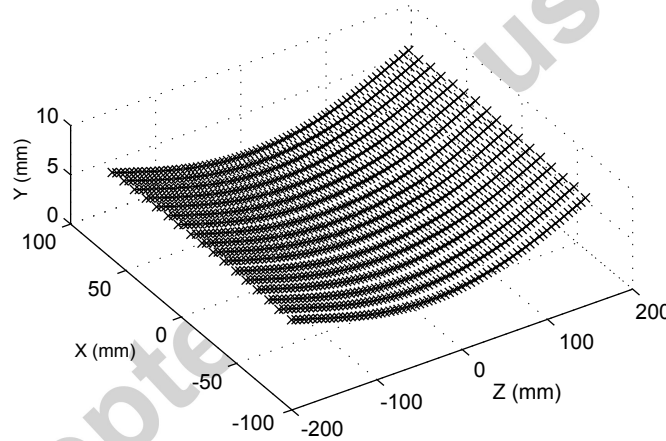


Fig. 17: Example of points, measured using the coordinate measuring machine, of a panel formed by springback-forming. (Test 2: plate:  $355\text{ mm} \times 170\text{ mm} \times 2.4\text{ mm}$ , stiffener:  $544\text{ mm} \times 17.6\text{ mm} \times 2.4\text{ mm}$ , initial applied stress  $\sigma^1 = 202.2\text{ MPa}$ ).

From these measures, and following the curvature characterization procedure of Section 3.2, Fig. 18 shows the transverse variation of the curvature radius of the three tests' plates. The maximum radial error is  $2\text{ mm}$ , which shows a good uniformity of the curvature radius of the plates' longitudinal fibers.

These experimental curves demonstrates clearly the feasibility of the process and that with springback-forming we can obtain a single-curved panel. It shows also that the results are repeatable. Indeed, if we consider Test 1 and Test 2, we observe that the geometrical parameters are practically identical and that the initial applied tensile stresses are close. Additionally, we note that the curvature radius decreases when we increase the initial tensile stress applied to the stiffener. This is coherent with the conclusion of the analytical and numerical model (Section 4.1).

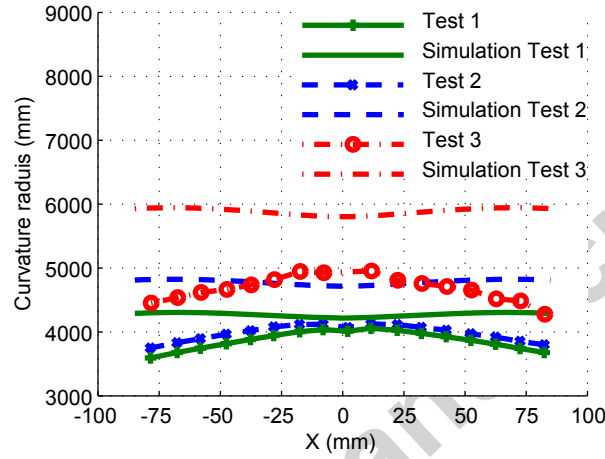


Fig. 18: Experimental and numerical transverse variation of longitudinal curvature radius of the three tests' panels, after forming by springback-forming (Test 1:  $\sigma^1 = 214.2 \text{ MPa}$ , Test 2:  $\sigma^1 = 202.2 \text{ MPa}$ , Test 3:  $\sigma^1 = 155.3 \text{ MPa}$ ).

On the other hand, using the developed numerical model, we simulated the three tests. Fig. 18 shows the transverse variation of the curvature radius of the panels. The radial error of the three simulations' results is inferior to  $0.2 \text{ mm}$ . To compare numerical and experimental results, Tab. 3 summarizes the curvature radius of the plate's longitudinal center fiber and the transverse dispersion of each test. We note that the numerical model overestimates the curvature radius and that the difference, between the two values, increases with the decreasing of the initial applied stress (from 4.9% in Test 1 to 15% in Test 3). As for the transverse dispersion, the numerical model underestimates it. This gap between the numerical and experimental result is because we ignored the effect of the assembly process. However, we are aware that welding introduces distortions and residual stresses that interact

515 with springback-forming process. To have a better quantitative estimation  
 516 of the results and more insight into these interactions, a model integrating  
 the simulation of laser beam welding should be developed.

	Test 1	Test 2	Test 3
Experimental curvature radius, $R_e$ (mm)	4010	4069	4927
Numerical curvature radius, $R_n$ (mm)	4218	4717	5810
Difference between $R_e$ and $R_n$ in percentage(%)	4.9	13.7	15.1
Experimental transverse dispersion (mm)	462	377	676
Numerical transverse dispersion (mm)	86	108	141

Table 3: Comparison of curvature radius of the plate's longitudinal center fiber and the transverse dispersion obtained numerically and experimentally from the three tests of springback-forming.

517

## 518 5. Conclusion

519 In this article, we have presented a forming process dedicated to stiffened  
 520 panels that we named springback-forming. It is based on the idea to apply a  
 521 tension on the stiffener before assembling it with the panel in a flat configu-  
 522 ration. The forming of the structure is achieved after releasing the stiffener's  
 523 tension. It has the merit of its reduced machines costs (as it uses mainly a  
 524 tension tool) and its adaptability to all panel sizes. By analyzing the process  
 525 steps, in the case of a plate with one stiffener, we showed that it is possible to  
 526 obtain a single-curved panel using the springback energy stored in the stiff-  
 527 ener. The concept of pre-stressing the stiffeners before the assembly could  
 528 be used in forming more complex panels.

529 To study the capabilities and the limitations of the process, an analytical  
 530 and a numerical model were developed. The analytical model is based on  
 531 Euler-Bernoulli beam theory. From this model we conclude that: – the more  
 532 the material is flexible, the smaller is the achievable curvature radius; – the  
 533 residual stresses in the structure are mainly longitudinal and the maximum  
 534 value is around the initial applied tensile stress. We also showed the existence  
 535 of minimum values of the curvature radius when analyzing its variation with  
 536 each geometrical parameter.

537 To have a more general tool to analyze the process, we have developed a  
 538 numerical simulation based on finite element method. To characterize the

539 panel's curvature after forming, we have defined three parameters: a cur-  
 540 vature radius of each longitudinal fiber of the plate, a radial error, and a  
 541 transverse dispersion evaluating the uniformity of the curvature in the entire  
 542 panel. The results of the numerical model, obtained through a parametrical  
 543 study, are in good agreement with those of the analytical one. This good  
 544 agreement makes the analytical model a quick tool to evaluate the effect of  
 545 the parameters on the process. On the other hand, the numerical model  
 546 allows the quantification of the uniformity of the panel's curvature radius.  
 547 According to the numerical simulations of the studied case, we conclude that  
 548 with the same initial applied force and above a minimum length ( $2m$  for  
 549 the reference configuration), the curvature radius becomes independent of  
 550 the structure's length. In contrast, the stiffener's height has a strong effect  
 551 on the process. Indeed, the curvature radius, increases from  $2m$  to more  
 552 than  $10m$  when the height changes from  $17.5mm$  to  $60mm$ . The stiffener  
 553 height could be a limitation to the minimum curvature radii achievable by the  
 554 process. As for the plate's width, it has a weaker effect than the stiffener's  
 555 height: the variation of the curvature radius is less than  $2m$  for a width  
 556 variation of  $1.8m$ . These conclusions are valid only for the considered struc-  
 557 ture. For other geometries, to define the achievable curvature radii and their  
 558 uniformity, similar curves to those presented in this article, should be plotted.  
 559 The experimental tests, carried out in this study, demonstrated that springback-  
 560 forming is capable of bending a single-curved panel and that its sensitivity  
 561 to initial tensile stress agrees qualitatively with the analytical and the nu-  
 562 merical model predictions. Hence, the process could be considered as a viable  
 563 alternative when choosing the most suitable process for a specific stiffened  
 564 panel. However, quantitatively the numerical model overestimates the pro-  
 565 duced curvature radius and underestimates the transverse dispersion of this  
 566 curvature radius. These differences are caused by laser beam welding used  
 567 as joining process. More experiments together with the integration in the  
 568 numerical model, of the distortions and the residual stress field introduced  
 569 by the joining process, should give more insight into its effect on springback-  
 570 forming.

## 571 References

- 572 Brewer, H., 1989. Age forming integrally stiffened, aluminum aerospace struc-  
 573 tures in an autoclave, in: Aircraft Design and Operations Meetings. Amer-  
 574 ican Institute of Aeronautics and Astronautics. doi:10.2514/6.1989-2087.

- 575 Davoodi, B., 2006. Etude du comportement quasi-statique et dynamique  
576 des matériaux métalliques à haute température—simulation numérique du  
577 formage à chaud. Ph.D. thesis. INSA de Rennes.
- 578 Gariépy, A., 2012. Finite element modelling of shot peening and peen forming  
579 processes and characterisation of peened AA2024–T351 aluminium alloy.  
580 Ph.D. thesis. Ecole Polytechnique de Montreal.
- 581 Holman, M.C., 1989. Autoclave age forming large aluminum aircraft  
582 panels. *Journal of Mechanical Working Technology* 20, pp. 477–488.  
583 doi:10.1016/0378-3804(89)90055-7.
- 584 Li, K., 1981. Using stress peen-forming process for integrally stiffened wing  
585 panels, in: 1st International Conference on Shot Peening, Paris, France.  
586 pp. 555–564.
- 587 Lin, J., Hoa, K.C., Dean, T.A., 2006. An integrated process for modelling  
588 of precipitation hardening and springback in creep age-forming. *Inter-  
589 national Journal of Machine Tools and Manufacture* 46, pp. 1266–1270.  
590 doi:10.1016/j.ijmachtools.2006.01.026.
- 591 Megson, T., 2010. *Introduction to Aircraft Structural Analysis* (Elsevier  
592 Aerospace Engineering). Butterworth-Heinemann.
- 593 Meyer, R., Reccius, H., Schulein, R., 1987. Shot peen-forming of nc-machined  
594 parts with integrated stringers using large balls, in: 3rd International Con-  
595 ferences on Shot Peening, Garmisch-Partenkirchen, Germany. pp. 327–334.
- 596 NASA-CR-124075, 1973. Isogrid design handbook. Technical Report. Mc-  
597 Donnell Douglas Astronautics Company.
- 598 Pettit, R.G., Wang, J.J., Toh, C., 2000. Validated feasibility study of  
599 integrally stiffened metallic fuselage panels for reducing manufacturing  
600 costs. Technical Report NASA/CR-2000-209342. National Aeronautics  
601 and Space Administration.
- 602 Takafumi, A., Shirou, K., Takahiro, N., Hiroyuki, T., Masakazu, S., 2004.  
603 Age forming technology for aircraft wing skin. *Materials Forum* 28, pp.  
604 202–207.

- 605 Toros, S., Ozturk, F., Kacar, I., 2008. Review of warm forming of aluminum-  
606 magnesium alloys. *Journal of Materials Processing Technology* 207, pp.  
607 1–12. doi:10.1016/j.jmatprotec.2008.03.057.
- 608 Wang, T., Platts, M., 2002. A computer-aided blank design method for the  
609 peen forming process. *Journal of Materials Processing Technology* 122, pp.  
610 374 – 380. doi:10.1016/S0924-0136(02)00049-3.
- 611 Yan, Y., Wan, M., Wang, H.B., 2009. FEM equivalent model for press  
612 bend forming of aircraft integral panel. *Transactions of Nonferrous Metals*  
613 *Society of China* 19, pp. 414 – 421. doi:10.1016/S1003-6326(08)60288-5.

614 **List of Figures**

615	1	The three steps of springback-forming. . . . .	5
616	(a)	Step 1: applying a tension on the stiffener. . . . .	5
617	(b)	Step 2: maintaining the stiffener's tension while assembling it with the plate. . . . .	5
618	(c)	Step 3: releasing the tension. . . . .	5
619	2	Geometrical parameters of the assembly's cross-section (stiffener and plate). . . . .	6
620	3	Example of residual stresses in the structure after its forming by springback-forming. . . . .	10
621	4	Hardening curve of the aluminum alloy 6056 <i>T4</i> at 20°C (Davoodi, 2006). . . . .	12
622	5	Example of mesh used in the finite element model. . . . .	13
623	6	Characterization of the longitudinal curvature of a panel. . . . .	14
624	(a)	Curvature characterization of a fiber in the plane $x = x_j$ . . . . .	14
625	(b)	Curvature radius of each longitudinal fiber. . . . .	14
626	7	Plate's nodes displacement after forming by springback-forming (plate: $4\text{ m} \times 170\text{ mm} \times 2.4\text{ mm}$ , stiffener: $4\text{ m} \times 17.5\text{ mm} \times 2.4\text{ mm}$ , initial applied stress $\sigma^1 = 300\text{ MPa}$ ). . . . .	15
627	(a)	Transverse displacement (X-direction) of the plate's nodes: $U_x$ . . . . .	15
628	(b)	Vertical displacement (Y-direction) of the plate's nodes: $U_y$ . . . . .	15
629	(c)	Longitudinal displacement (Z-direction) of the plate's nodes: $U_z$ (each half of the plate has its legend). . . . .	15
630	8	Curvature characterization of a panel after forming by springback-forming (plate: $4\text{ m} \times 170\text{ mm} \times 2.4\text{ mm}$ , stiffener: $4\text{ m} \times 17.5\text{ mm} \times 2.4\text{ mm}$ , initial applied stress $\sigma^1 = 300\text{ MPa}$ ). . . . .	16
631	(a)	Transverse variation of the longitudinal curvature radius. . . . .	16
632	(b)	Transverse variation of the radial error. . . . .	16
633	9	Longitudinal residual stress in the stiffener after forming. . . . .	16
634	10	Principal stresses in a structure's middle cross-section after forming. . . . .	17
635	(a)	Numerical principal stresses in the stiffener's middle cross-section. . . . .	17
636	(b)	Longitudinal residual stresses in the structure middle cross-section obtained by the analytical model. . . . .	17
637			
638			
639			
640			
641			
642			
643			
644			
645			
646			
647			
648			
649			
650			

651	11	Principal stresses in the central transverse section of the plate	
652		after forming. . . . .	17
653	(a)	Numerical principal stresses in the superior surface of	
654		the plate, in contact with the stiffener. . . . .	17
655	(b)	Numerical principal stresses in the inferior surface of the	
656		plate. . . . .	17
657	12	Von Mises stresses in the plate after its forming by springback-	
658		forming. . . . .	18
659	(a)	Plate's superior surface in contact with the stiffener. . .	18
660	(b)	Plate's inferior surface. . . . .	18
661	13	Variation of the plate's curvature radius with respect to the	
662		initial tensile stress applied to the stiffener. . . . .	19
663	14	Stiffener's height effect on the plate's curvature radius after	
664		forming. . . . .	20
665	(a)	Variation of the curvature radius of the plate's longitu-	
666		dinal center fiber with respect to the stiffener's height. .	20
667	(b)	Variation of the curvature radius's transverse dispersion	
668		( $\Delta R = R_{max} - R_{min}$ ) in the plate with respect to the	
669		stiffener's height. . . . .	20
670	15	Plate's width effect on its curvature radius after forming. . .	21
671	(a)	Variation of the curvature radius of the plate's longitu-	
672		dinal central fiber with respect to the plate's width. . .	21
673	(b)	Variation of curvature radius's transverse dispersion ( $\Delta R =$	
674		$R_{max} - R_{min}$ ) and the radial error in the plate with re-	
675		spect to the plate's width. . . . .	21
676	16	Structure's length effect on the plate's curvature radius after	
677		forming. . . . .	22
678	(a)	Variation of the curvature radius of the plate's central	
679		fiber with respect to the structure's length. . . . .	22
680	(b)	Variation of the curvature radius's transverse dispersion	
681		( $\Delta R = R_{max} - R_{min}$ ) in the plate with respect to the	
682		structure's length. . . . .	22
683	17	Example of points, measured using the coordinate measur-	
684		ing machine, of a panel formed by springback-forming. (Test	
685		2: plate: $355\text{ mm} \times 170\text{ mm} \times 2.4\text{ mm}$ , stiffener: $544\text{ mm} \times$	
686		$17.6\text{ mm} \times 2.4\text{ mm}$ , initial applied stress $\sigma^1 = 202.2\text{ MPa}$ ). . .	24



687	18	Experimental and numerical transverse variation of longitudinal curvature radius of the three tests' panels, after forming by springback-forming (Test 1: $\sigma^1 = 214.2 \text{ MPa}$ , Test 2: $\sigma^1 = 202.2 \text{ MPa}$ , Test 3: $\sigma^1 = 155.3 \text{ MPa}$ ). . . . .	25
-----	----	---	----

691 **List of Tables**

692	1	Initial loads and corresponding tensile stresses applied to the stiffener ( $4 \text{ m} \times 17.5 \text{ mm} \times 2.4 \text{ mm}$ ). . . . .	19
693			
694	2	Stiffeners height and the initial tensile stress applied to them in the three experimental tests of springback-forming. . . . .	23
695			
696	3	Comparison of curvature radius of the plate's longitudinal center fiber and the transverse dispersion obtained numerically and experimentally from the three tests of springback-forming. . . . .	26
697			
698			